

Grounding Beyond Detection: Enhancing Contextual Understanding in Embodied 3D Grounding

Yani Zhang^{1*}, Dongming Wu^{2*}, Hao Shi³, Yingfei Liu⁴,
Tiancai Wang⁴, Haoqiang Fan⁴, Xingping Dong^{1†}

¹School of Computer Science, Wuhan University

²Beijing Institute of Technology

³Tsinghua University ⁴Dexmal

{zebrazyn, xingpingdong}@whu.edu.com, wudongming97@gmail.com

Abstract

Embodied 3D grounding aims to localize target objects described in human instructions from ego-centric viewpoint. Most methods typically follow a two-stage paradigm where a trained 3D detector’s optimized backbone parameters are used to initialize a grounding model. In this study, we explore a fundamental question: Does embodied 3D grounding benefit enough from detection? To answer this question, we assess the grounding performance of detection models using predicted boxes filtered by the target category. Surprisingly, these detection models without any instruction-specific training outperform the grounding models explicitly trained with language instructions. This indicates that even category-level embodied 3D grounding may not be well resolved, let alone more fine-grained context-aware grounding. Motivated by this finding, we propose **DEGround**, which shares DETR queries as object representation for both **DE**tecton and **Grounding** and enables the grounding to benefit from basic category classification and box detection. Based on this framework, we further introduce a regional activation grounding module that highlights instruction-related regions and a query-wise modulation module that incorporates sentence-level semantic into the query representation, strengthening the context-aware understanding of language instructions. Remarkably, DEGround outperforms state-of-the-art model BIP3D by **7.52%** at overall accuracy on the EmbodiedScan validation set. The source code will be publicly available at <https://github.com/zyn213/DEGround>.

1 Introduction

Embodied 3D grounding [43] is an emerging task focused on perceiving 3D environments from a first-person perspective based on human instructions. This task has gained significant attention due to its promising applications in embodied agents that interact with and navigate real-world environments. Different from traditional 3D visual grounding (VG), which predicts 3D object bounding boxes using scene-level inputs such as reconstructed 3D point clouds or meshes [1; 9; 2; 49], embodied 3D grounding relies on an arbitrary numbers of ego-centric RGB-D images as inputs. The distinct nature of these inputs requires a rethinking of how to design a robust framework for comprehensively understanding and integrating RGB-D images as well as language instructions.

Existing embodied approaches [43; 54; 29] typically follow a two-stage paradigm, where a 3D detector is initially trained, and its well-optimized backbone parameters are later used to initialize the heterogeneous grounding model. In this setup, the detector and grounding model utilizes a shared

*Equal contribution. † Corresponding author.

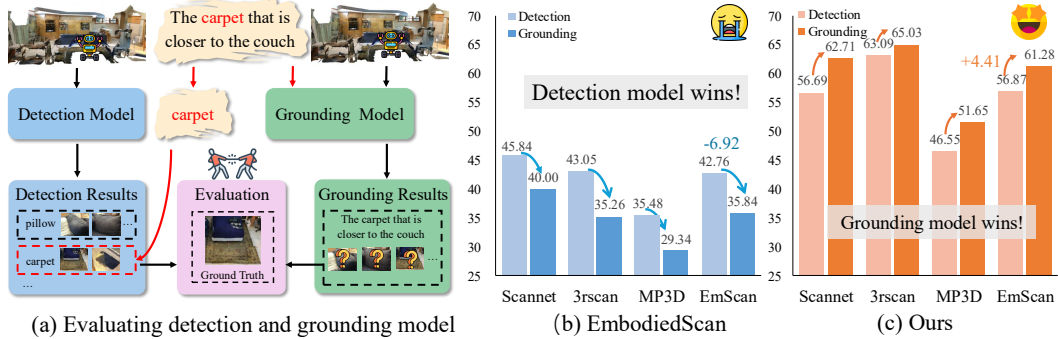


Figure 1: **Comparative evaluation of detection and grounding models on EmbodiedScan grounding benchmark.** (a) Detection models are evaluated by selecting predicted boxes based on target categories, while grounding models are assessed directly based on their predicted results. (b) EmbodiedScan [43] shows that *models that are not specifically trained with language instructions outperform grounding models explicitly trained with them on the grounding evaluation*. (c) Our model breaks up this performance limitation via enhancing category-level and context-aware understanding.

backbone while incorporating separate decoder heads. For instance, EmbodiedScan [43] modifies FCAF3D [36], an anchor-based method, for detection and uses a query-based architecture to predict grounding objects. This significant architectural shift raises a critical question: *Do the embodied 3D grounding models benefit enough from the pre-trained detection models?*

To answer this question, we assess detection and grounding models under identical conditions (i.e., the EmbodiedScan grounding benchmark). Specifically, due to the language instructions being templated-based, the category name of the target object can be extracted using predefined linguistic rules. Then we use the category label to collect prediction boxes from detection models for grounding evaluation, as shown in Fig. 1 (a). Interestingly, as shown in Fig. 1 (b), the detection models outperform the specialized grounding models in performance (e.g., 42.76 mAP vs. 35.84 mAP) 🤖. More similar comparisons (such as DenseGrounding [54]) can be found in the supplementary file.

Let us delve deeper into this phenomenon. Intuitively, evaluating all category-level box predictions from a detector on a single-object grounding task should introduce false positives and degrade performance compared to instruction-specific trained grounding models. However, the experimental results show the opposite: category-level predictions, even without any instruction-specific supervision, lead to higher grounding accuracy. It suggests that current grounding models cannot reliably perform basic category classification. This also poses a great challenge for understanding more complex instructions. In other words, if grounding models struggle to resolve basic category alignment, their capacity to interpret linguistic contextual relationships becomes even more questionable.

To address this, we introduce DEGround, a preliminary solution based on the DETection Transformer (DETR) [5] architecture which shares DETR queries as object representation for both detection and grounding. DEGround allows grounding to directly benefit from the strong category classification and bounding box regression capabilities of detection models. Language features are integrated into the shared queries to facilitate instruction-aware category learning.

To further enhance the visual-language understanding from a global context-aware perspective, we introduce two complementary components. 1) The Regional Activation Grounding (RAG) module considers region-level correlations between visual features and textual embeddings, promoting the model to focus on semantically relevant spatial regions. 2) The Query-wise Modulation (QIM) module injects global sentence-level semantics into the query representations, enriching the queries with contextual linguistic information. By integrating these components, DEGround effectively harnesses detection capabilities to achieve significant improvements (e.g., +4.41 mAP) in grounding performance 🤖, as shown in Fig. 1 (c).

In summary, our main contributions are four-fold:

- We identify a significant performance gap between existing embodied 3D detection and grounding models. To address this, we propose DEGround, which shares queries as object representations, preserving the strong classification capability of detection models.

- We introduce a novel regional activation grounding module that effectively highlights visual regions related to language descriptions. It complements query-based object grounding methods and integrates seamlessly with DEGround.
- We propose the query-wise modulation module that integrates global sentence-level semantics into the query representations, enhancing them with contextual linguistic information.
- We conduct extensive experiments on embodied perception benchmark EmbodiedScan. DEGround outperforms existing methods by a large margin, resulting in overall accuracy improvement of **7.52%** compared to state-of-the-art model BIP3D.

2 Related Work

2.1 3D Visual Grounding

3D visual grounding plays a vital role in a wide range of downstream applications, including robotic vision perception [15; 40; 35] and autonomous driving [4; 8]. Its core concept involves identifying and localizing target objects within 3D visual scenes based on natural language descriptions. A variety of datasets [1; 9; 2; 49] have been introduced to advance progress in this field. Prior approaches primarily employ two-stage methods [9; 26; 20; 48; 51; 47; 18; 28; 10; 45], where pre-trained object detectors are first applied to generate object proposals, and the target is subsequently selected from these proposals by designing various matching strategies. In recent years, one-stage methods have emerged as the dominant paradigm for 3D visual grounding [27; 19; 23; 7; 38; 41; 46; 50; 44]. For instance, MVT [27] employs a technique of rotating 3D scenes from various angles and encoding them to generate multi-view representations for bounding box prediction. While a previous study [16] explores the influence of natural language instructions, its focus is primarily on variations in language style, such as different accents or tones. In contrast, our work delves into studying the effectiveness of language instructions themselves. Moreover, most existing 3D visual grounding methods primarily focus on enhancing scene understanding using *scene-level* 3D point clouds or meshes. Differently, our research is centered on egocentric 3D visual grounding, leveraging RGB-D data to precisely locate objects in a more *sparse* input manner.

2.2 Multi-task learning with 3D Grounding

Leveraging 3D grounding and multi-task learning within a single framework has emerged as a highly active and trending research topic in embodied agent community. Most existing methods employ LLM-based frameworks [25; 24; 22; 11; 52], which convert inputs and outputs into visual or linguistic tokens to enable multi-task learning. For example, LEO [25] collects large-scale 3D vision-language datasets and builds an embodied multi-modal generalist agent that excels in perceiving, grounding, reasoning, planning, and acting in the 3D world. However, these methods still rely on an off-the-shelf 3D mask or box proposal module, requiring feeding these proposals into an LLM for grounding prediction. Different from them, PQ3D [55] introduces promptable queries within a DETR-like framework, offering a distinct and integrated solution. It integrates voxels, point clouds, and multi-view images into a unified 3D coordinate space through segment-level grouping, generating segmentation masks, bounding boxes, and captions as outputs. BIP3D [31] extends Grounding-DINO [32] by incorporating image features with 3D position encoding. However, this image-centric method lacks explicit 3D space modeling and relies heavily on extensive category label inputs for its detection task. In this work, we propose an elegant, effective, and plain DETR model designed for embodied 3D grounding, with the goal of unlocking the potential of language instructions.

3 Method

In this work, we introduce DEGround, which shares DETR queries as unified object representations for detection and grounding, enabling grounding to inherit detection’s classification and localization capabilities (§3.1). Additionally, we introduce a Regional Activation Grounding (RAG) module which highlights regions relevant to textual cues (§3.2) and a Query-wise Modulation (QIM) module which refines queries with sentence-level semantics (§3.3). The overall framework of our DEGround is shown in Fig. 2. In the following sections, we will delve into more model details.

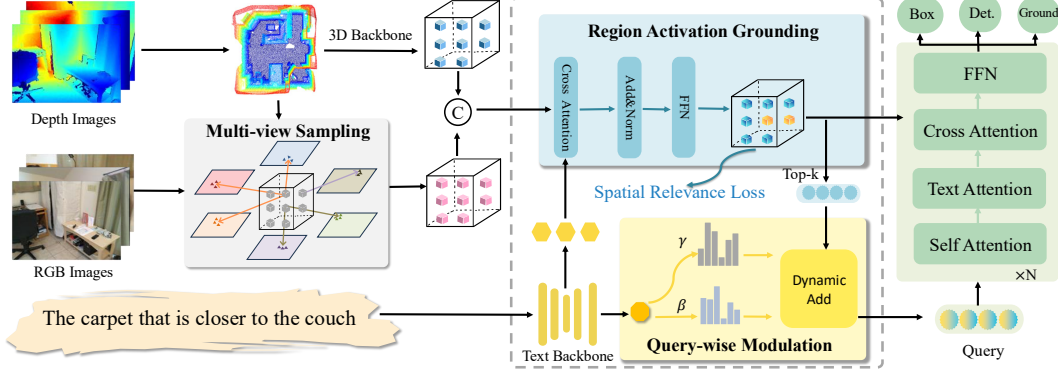


Figure 2: **The overall framework of our DEGround.** It shares DETR queries as object representation for basic category classification and instruction understanding. Besides, it includes a Region Activation Grounding (RAG) module for highlighting instruction-relevant regions and a Query-wise Modulation (QIM) module that dynamically modulates decoder queries with global linguistic context.

3.1 Overall Framework

Both grounding and detection tasks take multiple RGB-D image sequences as visual inputs and generate 3D bounding boxes as outputs. In the grounding task, the bounding box needs to be associated with an additional language description input that references it. Our overall framework uses a more advanced DETR-based architecture, which represents each object as a query.

Feature Extraction. Given V views of RGB-D inputs $\{(I_v, D_v)\}_{v=1}^V$, where each I_v represents an RGB image, and D_v corresponds to its depth map. We first reconstruct a sparse 3D scene representation by projecting the multi-view depth maps $\{D_v\}_{v=1}^V$ into world coordinates using their corresponding depth sensor intrinsic and extrinsic parameters. This process generates a pseudo-point cloud that preserves geometric fidelity to the physical environment. The pseudo-point cloud is then voxelized and encoded through a voxel encoder, producing multi-level 3D features $F_{3d} \in \mathbb{R}^{N \times C}$ and their 3D coordinates $F_{coord} \in \mathbb{R}^{N \times 3}$. Here, N is the voxel number, C represents the feature dimension, and we omit the level notion for simplicity. Concurrently, an image encoder is used to extract multi-scale 2D features from each RGB image, obtaining corresponding feature maps $F_{2d} \in \mathbb{R}^{H \times W \times C'}$ per view. Let L denote a language description with T words. We employ a pre-trained text backbone to extract text embeddings $F_{text} \in \mathbb{R}^{T \times C''}$. These three types of features are projected into the same feature dimension C via independent linear layers.

3D Feature Representation. Following the projection of all visual features into a unified embedding space, we construct a comprehensive 3D feature representation by hierarchically integrating two complementary feature streams: (i) 3D features F_{3d} , which encode the geometric structure of the scene, and (ii) 2D features F_{2d} , which provide rich semantic context from the RGB modalities. Here, each F_{2d} incorporates multi-view features, i.e., $F_{2d} = \{F_{v,2d}\}_{v=1}^V$.

To align 2D and 3D features, we first convert voxel indices to 3D point coordinates $P \in \mathbb{R}^{N \times 3}$ using the voxel size. These points are then projected onto multi-view image planes using camera parameters, and their corresponding 2D features are sampled via bilinear interpolation. Finally, the interpolated 2D features are concatenated with the 3D geometric features along the channel dimension, resulting in a fused visual representation F_{visual} that integrates both semantic and spatial information:

$$F_{visual} = \text{Concat}(F_{3d}, \text{Sample}(P, F_{2d})) \in \mathbb{R}^{N \times C}. \quad (1)$$

Query Sharing. Different from previous works [43; 54] that use two distinct decoder architectures, with detection relying on a convolution-based approach and grounding employing a transformer-based method, we propose query sharing strategy for both tasks. The overall pipeline is shown in Fig. 2. It accepts 3D features F_{visual} , text features F_{text} , and shared queries Q as inputs, and outputs 9-degree-of-freedom (9DoF) bounding boxes B , detection classification C^{det} and grounding classification C^{grd} . Formally, this process is written:

$$B, C^{det}, C^{grd} = \mathcal{F}^{Dec}(F_{visual}, F_{text}, Q), \quad (2)$$

where \mathcal{F}^{Dec} follows the architecture of Transformer decoder [5], including a stack of self-attention and cross-attention modules. Both the detection model and grounding model employ a standard cross-attention module to facilitate interaction between queries and 3D features F_{visual} . Additionally, the grounding model incorporates a cross-attention module to enhance text fusion at the query level. These three outputs use three independent MLP heads.

As for the shared query representation, both the detection and grounding models select Top-K point coordinates as anchors from F_{coord} , using their corresponding features as content queries. Each output box is denoted as a 9D vector $(x, y, z, l, w, h, \alpha, \beta, \gamma)$. Here, (x, y, z) are the 3D coordinates of an object, (l, w, h) are its dimensions, and (α, β, γ) represents its orientation angles. The detection classification is $C^{det} \in \mathbb{R}^{K \times C^{det}}$, where C^{det} is the category number. The grounding classification is $C \in \mathbb{R}^{N \times C^{grd}}$, where C^{grd} is the grounding number. In this way of shared queries, the more challenging grounding task can make full use of the basic category classification and box regression.

3.2 Regional Activation Grounding

Existing grounding methods [43; 54; 53; 29] predominantly incorporate language information only at the decoder stage via cross attention between queries and text features. However, such late-stage fusion limits the capacity to leverage fine-grained linguistic cues during earlier representation learning. As a result, the model struggles to focus on semantically relevant regions in complex scenes

To overcome this, we propose the Regional Activation Grounding (RAG) module, which explicitly highlights the regions that are semantically aligned with the language instruction. RAG consists of two key components: Text-driven Attention for cross-modal feature interaction and Spatial Relevance Loss to supervise region-level grounding. Details are provided in the following sections.

Text-driven Attention. Formally, we first employ a text-driven attention module \mathcal{F}^{att} to fuse the 3D visual feature F_{visual} with the linguistic representation F_{text} . This module computes attention weights based on the semantic relevance between the two modalities, allowing the model to highlight regions in the visual space that are most relevant to the given instruction, denote as F_{region} :

$$F_{region} = \mathcal{F}^{att}(Q = F_{visual}, K = F_{text}, V = F_{text}). \quad (3)$$

To preserve the original spatial information while enriching it with linguistic context, we adopt a residual connection by adding F_{region} back to the original 3D visual features:

$$F'_{region} = F_{visual} + F_{region} \in \mathbb{R}^{N \times C}, \quad (4)$$

where the final text-enhanced visual features F'_{region} can be a seamless insertion into the above overall framework. Finally, we will introduce an auxiliary spatial relevance loss to explicitly activate these related regions, further improving the grounding accuracy.

Spatial Relevance Loss. Specifically, a multi-layer perceptron (MLP) is employed to predict a spatial relevance score $S \in \mathbb{R}^{N \times 1}$ for each 3D point based on the fused feature representation F'_{region} .

$$S = \mathcal{F}^{MLP}(F'_{region}) \in \mathbb{R}^{N \times 1}. \quad (5)$$

The spatial relevance score represents the likelihood of a point belonging to a visual region associated with the given text. To supervise this prediction, we derive ground-truth labels $\hat{S} \in \mathbb{R}^{N \times 1}$ based on the annotated 3D bounding box: points located within the ground-truth region are assigned a label of 1, while those outside are assigned 0. The spatial relevance loss $\mathcal{L}_{spatial}$ is then computed using cross-entropy loss, comparing the predicted regional similarity scores S with these binary labels \hat{S} . By performing regional activation grounding, the text-aware regions are effectively activated. In the following section, we extend this idea to query-level activation with context-aware modulation.

3.3 Query-wise Modulation

While RAG facilitates global alignment between linguistic and visual modalities, it exhibits limited adaptability in modulating decoder queries according to task-specific semantic requirements during grounding. To address this limitation, we propose a Query-wise Modulation module that infuses linguistic cues into visual decoder queries via a lightweight yet expressive modulation mechanism.

As shown in Fig. 2, the core idea is to dynamically reshape the representation space of each decoder query according to the input instruction, thereby enhancing its semantic specificity and grounding

Table 1: **Comparison with state-of-the-art methods** on EmbodiedScan multi-view 3D detection benchmark. ‘MP3D’ refers to the Matterport3D sub-dataset in EmbodiedScan. The overall accuracy score is also reported on three sub-dataset: ScanNet, 3RScan, and MP3D. The best results are in bold.

Method	Overall	Head	Common	Tail	Small	Medium	Large	ScanNet	3RScan	MP3D
VoteNet [17]	5.18	10.87	2.41	2.07	0.16	5.30	5.99	9.90	7.69	3.82
ImVoxelNet [37]	8.08	3.11	7.05	3.73	0.06	7.95	9.02	11.91	2.17	5.24
FCAF3D [36]	13.86	22.89	9.61	8.75	2.90	13.90	10.91	21.35	17.02	9.78
EmbodiedScan [43]	15.22	24.95	10.81	9.48	3.28	15.24	10.95	22.66	18.25	10.91
BIP3D [31]	20.91	27.57	18.77	16.03	5.72	21.48	15.20	23.47	32.48	10.09
DEGround (Ours)	24.68	34.45	19.71	19.60	9.23	24.94	15.61	23.62	39.53	10.78

capacity. Concretely, given a sentence embedding $\mathbf{S} \in \mathbb{R}^C$, we employ two independent multi-layer perceptrons (MLPs), denoted as ξ_1 and ξ_2 , to generate modulation vectors $\beta, \gamma \in \mathbb{R}^C$:

$$\begin{aligned}\beta &= \xi_1(\mathbf{S}), \\ \gamma &= \xi_2(\mathbf{S}).\end{aligned}\tag{6}$$

These vectors encode the attention-to-vision and attention-to-language balance, respectively. Given an init set of M visual decoder queries $\mathbf{Q}_{vis} \in \mathbb{R}^{M \times C}$, the final language-aware queries $\mathbf{Q}_{mod} \in \mathbb{R}^{M \times C}$ are obtained via a feature-wise affine transformation:

$$\mathbf{Q}_{mod} = \beta \odot \mathbf{Q}_{vis} + \gamma \odot \mathbf{1}_M \mathbf{S},\tag{7}$$

where \odot denotes element-wise multiplication and $\mathbf{1}_M \in \mathbb{R}^{M \times 1}$ is a broadcast vector that replicates \mathbf{S} across all queries. This formulation enables each decoder query to be adaptively modulated by both visual and linguistic signals, thereby promoting more effective context-aware grounding.

3.4 Loss Function

We now introduce the loss function used to train our proposed DEGround in this part. To establish correspondences between predictions and ground-truth objects, we first find a bipartite graph matching which of the predicted objects fits the ground-truth. We search for a permutation of predictions by minimizing matching cost. The optimal assignment is then used to compute the detection loss:

$$\mathcal{L} = \lambda_{cls} \mathcal{L}_{cls} + \lambda_{box} \mathcal{L}_{box},\tag{8}$$

where \mathcal{L}_{cls} is the class-related loss implemented via focal loss [30], and \mathcal{L}_{box} is the box regression loss based on Wasserstein distance. λ_{cls} and λ_{box} are the corresponding hyper-parameters.

The same bipartite matching process is applied to align the predicted grounding boxes with the ground-truth annotations. The grounding loss includes three components: a focal classification loss \mathcal{L}_{ground} , a box regression loss \mathcal{L}_{box} (also based on Wasserstein distance), and a spatial relevance loss $\mathcal{L}_{spatial}$ introduced in §3.2. The full grounding objective is defined as:

$$\mathcal{L} = \lambda_{ground} \mathcal{L}_{ground} + \lambda_{box} \mathcal{L}_{box} + \lambda_{spatial} \mathcal{L}_{spatial}.\tag{9}$$

4 Experiments

4.1 Dataset and Evaluation Metric

Dataset. We evaluate our method on EmbodiedScan [43], a large-scale multi-modal egocentric 3D perception benchmark. It is composed of 4,633 high-quality scans from three well-know datasets: ScanNet (1,513 scans) [14], 3RScan (1,335 scans) [42], and Matterport3D (1,785 scans) [6]. The dataset does not include scene-level point clouds or meshes but instead provides continuous first-view RGB-D streams. For object detection, it features bounding boxes across 284 categories. For grounding task, it offers over 1 million language descriptions focusing on spatial relationships among objects. It surpasses previous datasets [13; 39; 6] by offering more than $10\times$ categories, prompts, and annotations, showing significant challenges.

Evaluation Metric. Following the evaluation protocol [43], we use overall accuracy, calculated based on mean Average Precision at an IoU threshold of 0.25, as the primary evaluation metric for

Table 2: **Comparison with state-of-the-art methods** on EmbodiedScan visual grounding benchmark. [†] denotes the result reproduced in our experiments. * represents the results obtained using deformable augmentations from the official repository, which is a concurrent work with ours. ‘-’ means unavailable. The best results are in bold.

Set	Method	Backbone	Overall	Easy	Hard	View-Dep	View-Indep	ScanNet	3RScan	MP3D
Mini	EmbodiedScan [†] [43]	ResNet-50	35.84	36.28	30.81	36.56	35.46	40.00	35.26	29.34
	DenseGrounding [54]	ResNet-50	41.34	41.95	34.38	40.89	42.19	44.45	41.08	33.72
	BIP3D [31]	Swin-T	45.79	46.22	40.91	45.93	45.71	48.94	46.61	37.36
	DEGround (Ours)	ResNet-50	61.28	61.76	55.84	62.95	60.39	62.71	65.03	51.65
Full	EmbodiedScan [43]	ResNet-50	39.41	40.12	31.45	40.21	38.96	41.99	41.53	30.29
	DenseGrounding [54]	ResNet-50	44.41	45.31	34.23	44.42	44.40	-	-	-
	BIP3D [31]	Swin-T	54.66	55.07	50.12	55.78	54.03	61.23	55.41	39.36
	BIP3D* [31]	Swin-T	61.36	61.88	55.58	62.43	60.76	66.96	62.75	46.92
	DEGround (Ours)	ResNet-50	62.18	62.76	55.70	63.56	61.40	63.02	65.98	52.95

Table 3: **Ablation studies of different components** on EmbodiedScan grounding validation set.

(a) Benefit of query sharing. ‘Ours-B’ refer to pre-trained backbones from our detection model, while ‘Ours’ uses the overall pre-trained detection model.

Pre-trained	Overall	Easy	Hard
-	7.62	7.74	6.20
EmbodiedScan	21.82	21.96	20.29
Ours-B	28.86	28.99	27.44
Ours	61.28	61.76	55.84

(c) Different query numbers.

Number	Overall	Easy	Hard
100	59.52	59.97	54.36
256	60.53	60.91	56.15
512	61.28	61.76	55.84

(b) Effective of our proposed Regional Activation Grounding module (RAG) and Query-wise Modulation (QIM) module.

RAG	QIM	Overall	Easy	Hard
-	-	59.90	60.37	54.57
✓	-	61.10	61.52	56.36
-	✓	60.63	61.06	55.73
✓	✓	61.28	61.76	55.84

(d) Different spatial relevance loss weights.

Weight	Overall	Easy	Hard
0.005	60.80	61.18	56.47
0.01	61.28	61.76	55.84
0.05	60.70	60.96	57.73

the detection task. We further report performance across three dimensions: category generalization (evaluated on head, common, and tail categories), object scale (segmented by small, medium, and large sizes), and scene-level generalization (across different scene types). For the 3D grounding task, overall accuracy also serves as the main evaluation metric. We additionally analyze performance with respect to instruction difficulty (based on the number of distractor objects), view dependency (whether the instruction contains directional cues), and sub-scene variations.

4.2 Implementation Details

Model. For feature extraction, we adopt ResNet50 [21] for 2D semantic features, Minkowski ResNet34 [12] for 3D geometric features, and RoBERTa [33] for textual features as the respective backbones. During the construction of 3D feature representations, all feature maps are projected into a consistent dimension of 256. The decoder is composed of six Transformer decoder layers, while the box, classification and grounding heads, built on top of the decoder, employ a Linear layer. We set the number of detection categories C^{det} to 284 and the grounding number C^{grd} to 1. The number of queries is 1024 for detection and 512 for grounding.

Training. We adopt the AdamW optimizer [34] for network training. Data augmentation includes random flipping and random rotation in 3D space. For 3D detection, the model is trained for 36 epochs on 8 Nvidia A100 GPUs with a batch size of 8. The learning rate is set to 1e-4 for the backbone and 1e-3 for the remaining parameters. Both loss weights λ_{cls} and λ_{box} are set to 1. For 3D grounding, the model is initialized from a 3D detection checkpoint and trained for 3 epochs with a learning rate of 5e-8. The loss weights are set as: $\lambda_{ground} = 1$, $\lambda_{box} = 1$, and $\lambda_{spatial} = 0.01$.

4.3 Comparison with State-of-The-Art

3D Grounding. We compare our model DEGround with existing methods [43; 54; 31] on the EmbodiedScan visual grounding benchmark, as shown in Table 2. Among them, DenseGrounding [54]

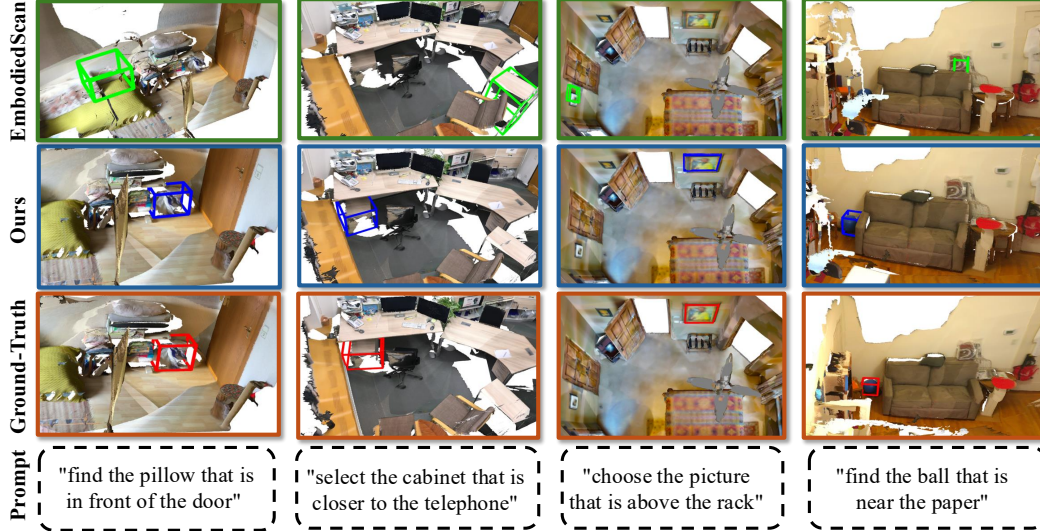


Figure 3: **Qualitative comparisons of our method and EmbodiedScan.** Our method demonstrates promising category-level and context-aware understanding performance.

ranked first place in the Multi-view 3D Visual Grounding Track of CVPR 2024 Autonomous Grand Challenge. Remarkably, DEGround outperforms all methods on both the full and mini validation dataset under all metrics, which demonstrating the superior effectiveness and robustness of our method. In specific, on the full validation dataset, DEGround with backbone ResNet-50 achieve **62.18%** on the overall accuracy metric. Compared to other models employing ResNet-50 as the backbone, DEGround surpasses the previous state-of-the-art DenseGrounding by **17.77%**. Furthermore, it outperforms BIP3D [31] with Swin-Tiny backbone by **7.52%** (62.18 vs. 54.66) on the overall accuracy metric. On the mini validation dataset, our method also establishes a new state-of-the-art.

3D Detection. In Table 1, we report results on EmbodiedScan visual detection benchmark. Previous methods usually rely on convolutional architectures due to the concerns about convergence challenges of transformer-based methods on large-scale datasets with over 200 object categories. Contrary to this assumption, our DETR-based framework achieves state-of-the-art performance and surpasses the previous SOTA method BIP3D by a substantial margin. The improvements range from 20.91% to 24.68%, demonstrating the superior effectiveness of our approach.

4.4 Ablation Studies

To offer a deep insight into our DEGround, we conduct ablation studies to analyze the effectiveness of each component. If not specialized, we report our performance on EmbodiedScan mini validation dataset using ResNet-50, with 1024 and 512 queries for detection and grounding, respectively.

Benefit of query sharing. To answer the aforementioned foundational question, we load backbone weights from two distinct detection models into our grounding model: EmbodiedScan detection model (i.e., “EmbodiedScan”) and our detection model (i.e., “Ours-B”), as shown in Tab. 3a. Both models are pre-trained on the EmbodiedScan detection task first. Compared to using complete pretrained detection weights, as shown in the last row, the two methods lead to 39.46% drop (61.28% \rightarrow 21.82%) and 32.42% drop (61.28% \rightarrow 28.86%), respectively. This indicates that our model benefits from the shared DETR query representations.

Effective of RAG and QIM. We also evaluate the effectiveness of the Regional Activation Grounding (RAG) and Query-wise Modulation (QIM) modules. As reported in Tab. 3b, incorporating either module independently results in performance improvements and combining both yields the best result. Notably, the RAG module contributes the most substantial gain, improving the baseline by 1.2%, thereby underscoring its effectiveness in enhancing grounding precision.

Grounding query numbers. It is also of interest to explore the impact of different query numbers. As shown in Tab. 3c, for grounding task, increasing the number of queries leads to consistent performance improvements, with mean Average Precision (mAP) gains of 1.01% and 0.75% observed

when increasing the number of queries from 100 to 256 and 512, respectively. However, this improvement comes at the cost of linearly increasing memory consumption. To achieve a favorable trade-off between accuracy and computational efficiency, we adopt 512 queries during training.

About spatial relevance loss. The spatial relevance loss is designed to refine the model’s ability to localize target regions. We explore different weights for this loss component to determine its impact on our model. As shown in Tab. 3d, a weighting of 0.01 achieves the optimal overall accuracy of 61.28%, outperforming both lower (0.005) and higher (0.05) weighting configurations. Based on these results, we set the region loss weight as $\lambda_{spatial} = 0.01$ throughout our experiments.

Detection query numbers. We further examine the effect of varying the number of detection queries on detection performance in Tab. 4. Specifically, we evaluate our model with 256, 512, and 1024 queries. The detection accuracy improves progressively from 22.48% with 256 queries to 23.20% with 512

Table 4: Ablation study on different detection query numbers on EmbodiedScan detection dataset.

Det. Query	Overall	Head	Common	Tail
256	22.48	32.11	19.19	15.63
512	23.20	33.13	19.30	16.72
1024	24.68	34.45	19.71	19.60

queries, and reaches 24.68% with 1024 queries. This trend indicates that increasing the number of detection queries enhances the model’s capacity to capture diverse object instances and improves its ability to localize targets more precisely. However, similar to the grounding task, the performance gains are accompanied by increased computational and memory costs. Finally, we adopt 1024 queries for all subsequent experiments to balance performance and efficiency.

4.5 Qualitative Results

We provide qualitative comparisons between our method and EmbodiedScan [43] across various scenarios, as shown in Fig. 3. Firstly, given the language prompt ‘find the ball that is near the paper’, EmbodiedScan fails to distinguish the target category and mistakenly selects a non-ball object, whereas our method accurately identifies and localizes the ball, showcasing stronger category-level classification capabilities. Secondly, with the prompt “select the cabinet that is closer to the telephone”, although EmbodiedScan identifies the correct category, it struggles with distractors of the same type and fails to locate the correct cabinet. In contrast, DEGround successfully distinguishes between similar instances and grounds the appropriate object. These results demonstrate that DEGround excels in both recognizing object categories and resolving fine-grained ambiguities. Additional comparative results are provided in the supplementary material.

In Fig. 4, we also visualize the regional similarity score generated by the RAG module. We first project these scores onto RGB images from different perspectives. Then render color-coded heatmaps according to the score value, where gray represents low similarity and red represents high similarity. The visualization clearly demonstrates the RAG module effectively highlights regions with higher text similarity. More visualizations can be found in the supplementary materials.

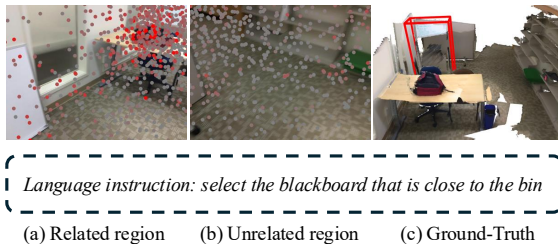


Figure 4: Visualization of regional similarity scores in RAG. RAG highlights higher relevant regions.

5 Conclusion

In this paper, we started with a fundamental question: Does embodied 3D grounding benefit from detection? Through evaluating current detection and grounding models, we uncovered an important insight: embodied 3D grounding in existing methods fails to effectively leverage detection. More specifically, this is because they cannot reliably perform basic category classification. To address this, we introduced DEGround, an elegant framework designed to share object query representations between the detection and grounding. This shared architecture allows the grounding model to capitalize on the strengths of basic category-level learning. Moreover, we introduced a regional activation grounding module to highlight target region and a query-wise modulation module that enhances query representations from a context-aware linguistic perspective. Our extensive experiments on the EmbodiedScan benchmark demonstrated that DEGround achieved state-of-the-art performance.

References

- [1] Achlioptas, P., Abdelreheem, A., Xia, F., Elhoseiny, M., Guibas, L.: Referit3d: Neural listeners for fine-grained 3d object identification in real-world scenes. In: ECCV (2020) 1, 3
- [2] Azuma, D., Miyanishi, T., Kurita, S., Kawanabe, M.: Scanqa: 3d question answering for spatial scene understanding. In: CVPR (2022) 1, 3
- [3] Baruch, G., Chen, Z., Dehghan, A., Dimry, T., Feigin, Y., Fu, P., Gebauer, T., Joffe, B., Kurz, D., Schwartz, A., et al.: Arkitscenes: A diverse real-world dataset for 3d indoor scene understanding using mobile rgb-d data. arXiv (2021) 13
- [4] Caesar, H., Bankiti, V., Lang, A.H., Vora, S., Liong, V.E., Xu, Q., Krishnan, A., Pan, Y., Baldan, G., Beijbom, O.: nuscenes: A multimodal dataset for autonomous driving. In: CVPR (2020) 3
- [5] Carion, N., Massa, F., Synnaeve, G., Usunier, N., Kirillov, A., Zagoruyko, S.: End-to-end object detection with transformers. In: ECCV (2020) 2, 5
- [6] Chang, A., Dai, A., Funkhouser, T., Halber, M., Niessner, M., Savva, M., Song, S., Zeng, A., Zhang, Y.: Matterport3d: Learning from rgb-d data in indoor environments. arXiv preprint arXiv:1709.06158 (2017) 6
- [7] Chang, C.P., Wang, S., Pagani, A., Stricker, D.: Mikasa: Multi-key-anchor & scene-aware transformer for 3d visual grounding. In: CVPR (2024) 3
- [8] Chen, C., Jain, U., Schissler, C., Gari, S.V.A., Al-Halah, Z., Ithapu, V.K., Robinson, P., Grauman, K.: Soundspaces: Audio-visual navigation in 3d environments. In: ECCV (2020) 3
- [9] Chen, D.Z., Chang, A.X., Nießner, M.: Scanrefer: 3d object localization in rgb-d scans using natural language. In: ECCV (2020) 1, 3
- [10] Chen, S., Guhur, P.L., Tapaswi, M., Schmid, C., Laptev, I.: Language conditioned spatial relation reasoning for 3d object grounding. NeurIPS (2022) 3
- [11] Chen, Y., Yang, S., Huang, H., Wang, T., Xu, R., Lyu, R., Lin, D., Pang, J.: Grounded 3d-llm with referent tokens. arXiv preprint arXiv:2405.10370 (2024) 3
- [12] Choy, C., Gwak, J., Savarese, S.: 4d spatio-temporal convnets: Minkowski convolutional neural networks. In: CVPR (2019) 7
- [13] Couprie, C., Farabet, C., Najman, L., LeCun, Y.: Indoor semantic segmentation using depth information. arXiv preprint arXiv:1301.3572 (2013) 6
- [14] Dai, A., Chang, A.X., Savva, M., Halber, M., Funkhouser, T., Nießner, M.: Scannet: Richly-annotated 3d reconstructions of indoor scenes. In: CVPR (2017) 6
- [15] Deitke, M., VanderBilt, E., Herrasti, A., Weihs, L., Ehsani, K., Salvador, J., Han, W., Kolve, E., Kembhavi, A., Mottaghi, R.: Procthor: Large-scale embodied ai using procedural generation. NeurIPS (2022) 3
- [16] Deng, W., Yang, J., Ding, R., Liu, J., Li, Y., Qi, X., Ngai, E.: Can 3d vision-language models truly understand natural language? arXiv preprint arXiv:2403.14760 (2024) 3
- [17] Ding, Z., Han, X., Niethammer, M.: Votenet: A deep learning label fusion method for multi-atlas segmentation. In: MICCAI (2019) 6
- [18] Feng, M., Li, Z., Li, Q., Zhang, L., Zhang, X., Zhu, G., Zhang, H., Wang, Y., Mian, A.: Free-form description guided 3d visual graph network for object grounding in point cloud. In: ICCV (2021) 3
- [19] Guo, Z., Tang, Y., Zhang, R., Wang, D., Wang, Z., Zhao, B., Li, X.: Viewrefer: Grasp the multi-view knowledge for 3d visual grounding. In: ICCV (2023) 3
- [20] He, D., Zhao, Y., Luo, J., Hui, T., Huang, S., Zhang, A., Liu, S.: Transrefer3d: Entity-and-relation aware transformer for fine-grained 3d visual grounding. In: ACM MM (2021) 3

- [21] He, K., Zhang, X., Ren, S., Sun, J.: Deep residual learning for image recognition. In: CVPR (2016) 7
- [22] Hong, Y., Zhen, H., Chen, P., Zheng, S., Du, Y., Chen, Z., Gan, C.: 3d-llm: Injecting the 3d world into large language models. NeurIPS (2023) 3
- [23] Hsu, J., Mao, J., Wu, J.: Ns3d: Neuro-symbolic grounding of 3d objects and relations. In: CVPR (2023) 3
- [24] Huang, H., Chen, Y., Wang, Z., Huang, R., Xu, R., Wang, T., Liu, L., Cheng, X., Zhao, Y., Pang, J., et al.: Chat-scene: Bridging 3d scene and large language models with object identifiers. In: NeurIPS (2024) 3
- [25] Huang, J., Yong, S., Ma, X., Linghu, X., Li, P., Wang, Y., Li, Q., Zhu, S.C., Jia, B., Huang, S.: An embodied generalist agent in 3d world. arXiv preprint arXiv:2311.12871 (2023) 3, 13
- [26] Huang, P.H., Lee, H.H., Chen, H.T., Liu, T.L.: Text-guided graph neural networks for referring 3d instance segmentation. In: AAAI (2021) 3
- [27] Huang, S., Chen, Y., Jia, J., Wang, L.: Multi-view transformer for 3d visual grounding. In: CVPR (2022) 3
- [28] Jain, A., Gkanatsios, N., Mediratta, I., Fragkiadaki, K.: Bottom up top down detection transformers for language grounding in images and point clouds. In: ECCV (2022) 3
- [29] Liang, C., Li, B., Zhou, Z., Wang, L., He, P., Hu, L., Wang, H.: Spatioawaregrounding3d: A spatio aware model for improving 3d vision grouding. In: Autonomous Grand Challenge CVPR 2024 Workshop. vol. 6 (2024) 1, 5, 13
- [30] Lin, T.Y., Goyal, P., Girshick, R., He, K., Dollár, P.: Focal loss for dense object detection. In: Proceedings of the IEEE international conference on computer vision. pp. 2980–2988 (2017) 6
- [31] Lin, X., Lin, T., Huang, L., Xie, H., Su, Z.: Bip3d: Bridging 2d images and 3d perception for embodied intelligence. arXiv preprint arXiv:2411.14869 (2024) 3, 6, 7, 8, 13
- [32] Liu, S., Zeng, Z., Ren, T., Li, F., Zhang, H., Yang, J., Jiang, Q., Li, C., Yang, J., Su, H., et al.: Grounding dino: Marrying dino with grounded pre-training for open-set object detection. In: ECCV (2024) 3
- [33] Liu, Y., Ott, M., Goyal, N., Du, J., Joshi, M., Chen, D., Levy, O., Lewis, M., Zettlemoyer, L., Stoyanov, V.: Roberta: A robustly optimized bert pretraining approach. arXiv preprint arXiv:1907.11692 (2019) 7
- [34] Loshchilov, I., Hutter, F.: Decoupled weight decay regularization. ICLR (2017) 7
- [35] Luo, J., Fu, J., Kong, X., Gao, C., Ren, H., Shen, H., Xia, H., Liu, S.: 3d-sps: Single-stage 3d visual grounding via referred point progressive selection. In: CVPR (2022) 3
- [36] Rukhovich, D., Vorontsova, A., Konushin, A.: Fcaf3d: Fully convolutional anchor-free 3d object detection. In: ECCV (2022) 2, 6
- [37] Rukhovich, D., Vorontsova, A., Konushin, A.: Imvoxelnet: Image to voxels projection for monocular and multi-view general-purpose 3d object detection. In: WACV (2022) 6
- [38] Shi, X., Wu, Z., Lee, S.: Aware visual grounding in 3d scenes. In: CVPR (2024) 3
- [39] Song, S., Lichtenberg, S.P., Xiao, J.: Sun rgb-d: A rgb-d scene understanding benchmark suite. In: CVPR (2015) 6
- [40] Tian, X., Jiang, T., Yun, L., Mao, Y., Yang, H., Wang, Y., Wang, Y., Zhao, H.: Occ3d: A large-scale 3d occupancy prediction benchmark for autonomous driving. NeurIPS (2023) 3
- [41] Unal, O., Sakaridis, C., Saha, S., Van Gool, L.: Four ways to improve verbo-visual fusion for dense 3d visual grounding. In: ECCV (2024) 3

- [42] Wald, J., Avetisyan, A., Navab, N., Tombari, F., Nießner, M.: Rio: 3d object instance re-localization in changing indoor environments. In: ICCV (2019) 6
- [43] Wang, T., Mao, X., Zhu, C., Xu, R., Lyu, R., Li, P., Chen, X., Zhang, W., Chen, K., Xue, T., et al.: Embodiedscan: A holistic multi-modal 3d perception suite towards embodied ai. In: CVPR (2024) 1, 2, 4, 5, 6, 7, 9, 13
- [44] Wang, Y., Li, Y., Wang, S.: G³-lq: Marrying hyperbolic alignment with explicit semantic-geometric modeling for 3d visual grounding. In: CVPR (2024) 3
- [45] Wu, C., Ji, J., Wang, H., Ma, Y., Huang, Y., Luo, G., Fei, H., Sun, X., Ji, R., et al.: Rg-san: Rule-guided spatial awareness network for end-to-end 3d referring expression segmentation. *NeurIPS* 37, 110972–110999 (2024) 3
- [46] Xu, C., Han, Y., Xu, R., Hui, L., Xie, J., Yang, J.: Multi-attribute interactions matter for 3d visual grounding. In: CVPR (2024) 3
- [47] Yang, Z., Zhang, S., Wang, L., Luo, J.: Sat: 2d semantics assisted training for 3d visual grounding. In: ICCV (2021) 3
- [48] Yuan, Z., Yan, X., Liao, Y., Zhang, R., Wang, S., Li, Z., Cui, S.: Instancerefer: Cooperative holistic understanding for visual grounding on point clouds through instance multi-level contextual referring. In: ICCV (2021) 3
- [49] Zhang, Y., Gong, Z., Chang, A.X.: Multi3drefer: Grounding text description to multiple 3d objects. In: ICCV (2023) 1, 3
- [50] Zhang, Y., Luo, H., Lei, Y.: Towards clip-driven language-free 3d visual grounding via 2d-3d relational enhancement and consistency. In: CVPR (2024) 3
- [51] Zhao, L., Cai, D., Sheng, L., Xu, D.: 3dvg-transformer: Relation modeling for visual grounding on point clouds. In: ICCV (2021) 3
- [52] Zheng, D., Huang, S., Zhao, L., Zhong, Y., Wang, L.: Towards learning a generalist model for embodied navigation. In: CVPR (2024) 3
- [53] Zheng, H., Shi, H., Chng, Y.X., Huang, R., Ni, Z., Tan, T., Peng, Q., Weng, Y., Shi, Z., Huang, G.: Denseg: Alleviating vision-language feature sparsity in multi-view 3d visual grounding. In: Autonomous Grand Challenge CVPR 2024 Workshop. vol. 2, p. 6 (2024) 5
- [54] Zheng, H., Shi, H., Peng, Q., Chng, Y.X., Huang, R., Weng, Y., Huang, G., et al.: Densegrounding: Improving dense language-vision semantics for ego-centric 3d visual grounding. In: ICLR (2025) 1, 2, 4, 5, 7, 13
- [55] Zhu, Z., Zhang, Z., Ma, X., Niu, X., Chen, Y., Jia, B., Deng, Z., Huang, S., Li, Q.: Unifying 3d vision-language understanding via promptable queries. In: ECCV (2024) 3

Appendix

A Comparative Evaluation of Detection and Grounding Models

In Fig. 5, we present the grounding performance of more detection and grounding models [25; 54] on the EmbodiedScan grounding benchmark [43]. For fairness, all detection models do not use NMS post-processing. Results on both EmbodiedScan [25] and DenseGrounding [54] indicate that category-level predictions, even without instruction-specific supervision, yield higher grounding accuracy. This further suggests that current grounding models struggle with reliable category classification. Our method, DEGround, addresses this by sharing DETR queries as object representations for both detection and grounding, enabling grounding to directly benefit from the strong category classification and bounding box regression capabilities of detection models.

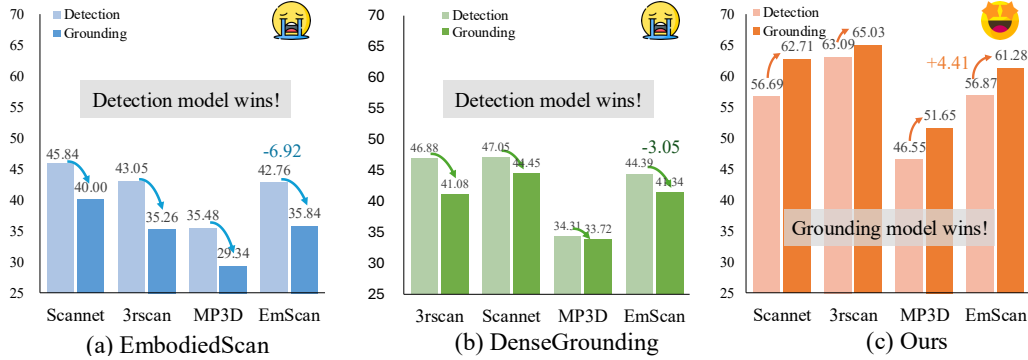


Figure 5: Evaluation of detection and grounding models on EmbodiedScan grounding.

B Results on Test Leaderboard

We also compare our DEGround with existing methods on the EmbodiedScan visual grounding test leaderboard, which uses a non-public test set maintained by the official benchmark. As shown in Tab. 5, our method achieves state-of-the-art performance, even when compared to methods employing stronger backbones. The performance gain at the IOU@0.25 threshold is relatively small, which may be attributed to BIP3D [31] being trained with additional external data [3]. However, when the IOU threshold is raised to 0.5, our model demonstrates a more significant advantage, indicating its superior localization precision under stricter evaluation criteria.

Table 5: Comparison with state-of-the-art methods on EmbodiedScan grounding test leaderboard.

Method	Backbone	Overall _{0.25}	Easy _{0.25}	Hard _{0.25}	Overall _{0.5}	Easy _{0.5}	Hard _{0.5}
EmbodiedScan [43]	ResNet-50	39.67	40.52	30.24	16.35	16.71	12.37
SAG3d [29]	ResNet-50	46.92	47.72	38.03	20.38	20.91	14.49
DenseGrounding [54]	ResNet-50	59.59	60.39	50.81	34.72	35.46	26.56
BIP3D [31]	Swin-T	70.53	71.22	62.91	39.69	40.40	31.77
DEGround (Ours)	ResNet-50	70.56	71.42	60.99	42.04	42.65	35.18

C More Qualitative Comparisons

We provide additional qualitative comparisons between DEGround and EmbodiedScan [43] in Fig 6. DEGround demonstrates strong capability in accurately grounding target objects across both simple and complex prompts. In contrast, EmbodiedScan struggles with same-category distractors and even fails basic category recognition. For example, it predicts a non-window object for the prompt ‘find the window that is farthest from the bathtub’. This highlights its limited categorization ability let alone inadequate understanding of language instructions. These qualitative results further demonstrate the effectiveness of DEGround in understanding instructions and achieving precise grounding.

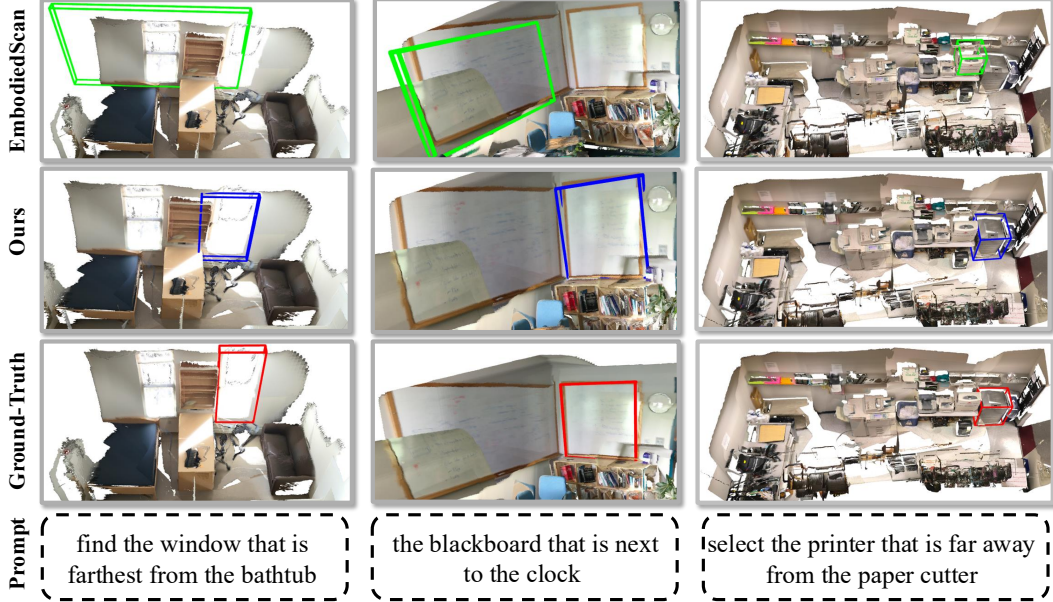


Figure 6: More qualitative comparisons of our method and EmbodiedScan.

D More visualizations of RAG

More visualizations of regional similarity scores from the RAG can be found in Fig 7. RAG effectively highlights regions that better align with the textual descriptions. For instance, in the first row, the desk farthest from the blackboard receives a higher score than those closer to it. These visualizations demonstrate the effectiveness of the RAG module in capturing text-relevant spatial regions.

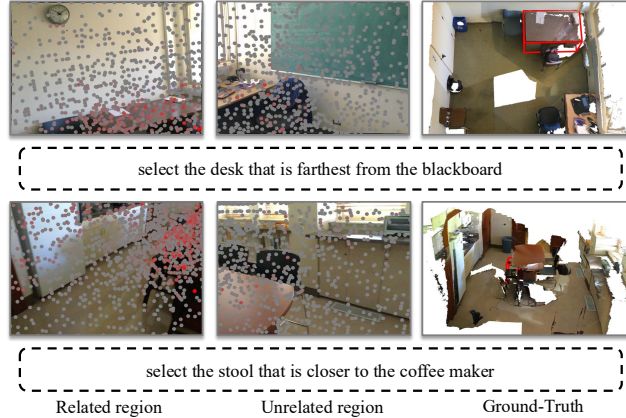


Figure 7: More visualizations of regional similarity scores in RAG.

E Discussion

Limitations. The proposed framework, DEGround, demonstrates strong embodied 3D understanding and achieves excellent grounding performance. However, there are some potential limitations. For instance, the current architecture assumes full-scene observation and lacks an explicit mechanism for early stopping during exploration. We believe that designing goal-aware policies or integrating active perception strategies to enable efficient search remains an interesting direction for future work.

Real World Impact. While DEGround could potentially be misused for privacy-invasive applications such as unauthorized object localization in personal environments, we consider the embodied 3D grounding task itself to be application-neutral. When applied responsibly, it enables positive use cases in assistive robotics, human-robot interaction, and context-aware augmented reality systems.